

**Self-propulsion of a periodically forced shape-deforming submillimeter gas bubble**Stephen J. Shaw *Department of Applied Mathematics, School of Mathematics and Physics, Xi'an Jiaotong-Liverpool University, 111 Ren Ai Road, Dushu Lake Higher Education Town, Suzhou, Jiangsu 215123, People's Republic of China*

(Received 25 March 2024; accepted 8 May 2024; published 24 May 2024)

The self-propulsion (translational instability) of a gas bubble in a liquid undergoing parametrically induced axisymmetric shape distortion due to being forced by a temporally sinusoidal, spatially constant acoustic field is investigated. Employing a model which accounts for the nonlinear coupling between the spherical oscillations, the axial translation and shape deformation of the bubble, the parametric excitation of two neighboring shape modes by the fundamental resonance, at the same driving frequency is studied. It is shown that provided pertinent driving pressure threshold values are exceeded, the respective shape modes are excited on different timescales. The growth of the shape mode on the faster timescale saturates giving rise to sustained constant amplitude oscillations, while the growth of the shape mode on the slower timescale is both modulated and unbounded. During the growth of the second shape mode, growing, oscillatory bubble translation is also observed.

DOI: [10.1103/PhysRevE.109.055107](https://doi.org/10.1103/PhysRevE.109.055107)**I. INTRODUCTION**

The spherically symmetric oscillations of a gas bubble in a liquid being forced by a periodic pressure field are susceptible to parametric instabilities which, for a sufficiently large driving pressure, will cause this symmetry to break, giving rise to distinct and possibly complex surface shape oscillation patterns. To model such patterns the shape distortion is often expressed as an infinite sum of spherical harmonics, reducing to Legendre polynomials in axisymmetry, the amplitudes of which are referred to as shape modes and which have their own distinctive oscillation frequencies [1]. In experimental studies of shape deformation, an often encountered difficulty is due to translational instability. Though the bubble can be seen deforming in shape, detailed and precise measurement of the resultant deformation can prove difficult due to this positional instability which causes the initially stationary bubble to move, often in a random or chaotic manner. This erratic motion, first reported by Gaines [2] and often referred to as bubble “dancing,” is a phenomenon which not only impedes the experimental observation of the shape deformation but also the potential for the controlled manipulation and propulsion of the gas bubbles [3]. A link between the observed shape deformation and the resultant motion of the bubble was first suggested by Strasberg and Benjamin [4] and Benjamin and Strasberg [5] with more conclusive experimental evidence being provided by Crum and Eller [6], but an explanation for how this is achieved was first provided by Benjamin and Ellis [7]. Building on the previous theoretical work of Benjamin and Strasberg [5] and Saffman [8], a key conclusion of the work of Ref. [7] is that the interaction between two neighboring shape modes can result in bubble self-movement. Benjamin and Ellis [7] considered both axisymmetric and asymmetric shape deformation deriving an equation for the resultant bubble velocity. However, this expression requires the temporal evolution of the shape modes to be already known and does not explain how the motion can become

chaotic. Clearly, therefore, under this proposed mechanism it is important to determine under what circumstances neighboring shape modes can become excited, the nature of their resultant behavior and whether their interaction is sufficiently strong to yield observable bubble motion, let alone chaotic motion.

Deriving pertinent amplitude equations for the nonlinear resonance between two neighboring shape modes and the volume mode using a multiple timescale method, Mei and Zhou [9] demonstrated the possibility of chaotic shape mode oscillations, but their model did not include direct interactions between the shape modes. Under the assumption that the driving pressure was in approximately a 2:1 resonance (often referred to as the fundamental or first harmonic resonance) with two neighboring shape modes, but the driving frequency was not near a resonance of the volume mode, Feng and Leal [10] derived coupled amplitude equations for the evolution of the volume mode and the two neighboring shape modes. Doinikov [11] applied perturbation techniques to derive a system of coupled evolution equations in the volume mode, the translation mode, and the shape modes in which the bubble axial speed and the shape oscillations were considered small but no restriction was placed on the volume mode. The presented system of equations included all interaction terms to second order in the shape modes and translation in an axisymmetric geometry. Both Feng and Leal [10] and Doinikov [11] confirmed the potential for bubble self-propulsion through the interaction of parametrically excited, neighboring shape modes.

Experimentally, the possibility of sustained, finite amplitude, stable shape mode oscillations as a consequence of parametric instability is well established but the link with nonlinear shape mode interactions has only recently been elucidated [12–17]. Provided a threshold driving pressure is exceeded, the exact value being problem dependent, the parametrically excited shape mode will initially grow exponentially, but this growth can saturate as a consequence of

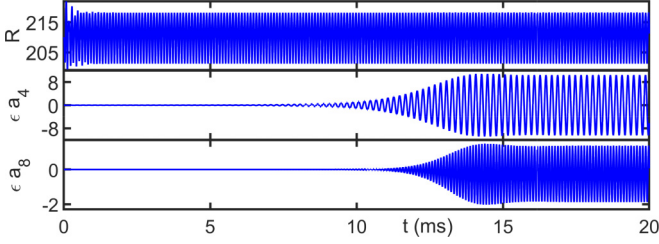


FIG. 1. Volume mode and shape mode oscillations for  $R_0 = 210 \mu\text{m}$ ,  $p_a = 10 \text{ kPa}$ , and  $f_d = 10 \text{ kHz}$ .

energy being passed to other shape modes via nonlinear shape mode interactions together with viscous damping. Though the amplitude of the resultant oscillations of the shape modes can be small relative to the parametrically excited shape mode, it is sufficient to yield stable shape mode oscillations. In this context, translation is then possible as a consequence of the parametrically excited shape mode interacting with a nonlinearly excited neighboring shape mode, provided the parametrically excited shape mode is odd, but generally the predicted movement, though oscillatory, is relatively small [12,13,15,17]. For example, in Shaw (2017), for a bubble with an initial radius of  $144 \mu\text{m}$  driven at  $10 \text{ kHz}$  and with a driving strength of  $13 \text{ kPa}$ , the predicted displacement is oscillatory with an amplitude of approximately  $0.5 \mu\text{m}$ . In order to observe larger, even chaotic motion, a more likely scenario is that two neighboring shape modes are both excited parametrically with sufficiently large amplitudes that their resultant interaction leads to observable bubble translation. It is this case that we consider here, extending the work of Feng and Leal [10] and Doinikov [11]. We restrict attention to cases where both of the neighboring shape modes are excited by the same driving frequency and by the fundamental parametric resonance, but place no restrictions on any potential volume resonances. We seek to determine the importance of sustained, finite amplitude shape mode oscillations, if they occur, in any resultant bubble self-propulsion. We note that as the order of the shape mode increases, the natural frequency values of two neighboring shape modes get closer together and therefore the potential for two neighboring shape modes to be parametrically excited by the same driving frequency increases. Examples of potential overlap regions can be found in Refs. [10,17–19].

## II. PROBLEM SETUP

Consider a single free gas bubble submerged in a liquid being forced by a temporally sinusoidal pressure field whose wavelength is much larger than the bubble diameter and therefore at any time  $t$  is assumed to act uniformly over the bubble. The evolution of the bubble surface is defined by the equation

$$S(r, \theta, t) = r - R(t) - \sum_{n=2}^{\infty} \epsilon a_n(t) P_n(\cos \theta) = 0, \quad (1)$$

where  $r$  and  $\theta$  are axisymmetric spherical polar coordinates,  $P_n(\cos \theta)$  denotes the Legendre polynomial of degree  $n$ , and  $\epsilon a_n(t)$  is the  $n$ th order shape mode. The parameter  $\epsilon$  is assumed both small and dimensionless such that

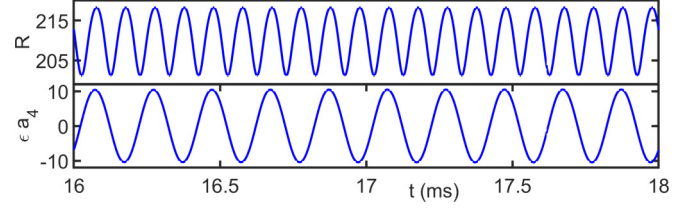


FIG. 2. Volume mode and  $n = 4$  shape mode oscillations for  $R_0 = 210 \mu\text{m}$ ,  $p_a = 10 \text{ kPa}$ , and  $f_d = 10 \text{ kHz}$  on an enhanced timescale.

$\epsilon a_n(t)/R_0 \ll 1$ ,  $R_0$  being the initial bubble radius. To model the resultant dynamics we employ the set of coupled ordinary differential equations presented by Shaw [15], modified here to include thermal effects inside the bubble and heat dissipation across the bubble surface. This system was derived using a Lagrangian/Hamiltonian energy approach combined with perturbation analysis in the small parameter  $\epsilon$  [20,21], modified to include (weak) compressibility effects [15]. In Shaw [15] it was shown that in the initial stages of the volume mode oscillations compressible effects cause the volume mode to reach a steady state on a faster timescale while a combination of viscous damping and nonlinear shape mode interactions result in the saturation of the growth of shape modes [12,13,15–17].

A condensed form of the dynamical equations governing the volume mode  $R(t)$ , the translation mode  $\epsilon z(t)$ , and the shape modes  $\epsilon a_n(t)$ ,  $n \geq 2$  is given in the Appendix. This system is solved numerically [15], subject to the following initial conditions:

$$\begin{aligned} R(0) &= R_0 \mu\text{m}, & \epsilon z(0) &= \epsilon a_n(0) = 1 \text{ nm}, \\ \dot{R}(0) &= \epsilon \dot{z}(0) = \epsilon \dot{a}_n(0) = 0. \end{aligned} \quad (2)$$

For the bubble sizes considered in this work, Prosperetti [22], Prosperetti *et al* [23], Prosperetti [24], Zhou and Prosperetti [25], for example, observe that thermal dissipation is a dominant dissipation mechanism. Therefore, to account for temperature variations within the bubble and thermal dissipation across the gas/liquid interface, the temporal evolution of the pressure inside the bubble is calculated using the bi-quadratic method presented in Zhou and Prosperetti [25]. In terms of the scaled coordinate  $y = r/R$ , the absolute gas temperature  $T$  inside the bubble is assumed to have the explicit form [25]

$$T(y, t) = T_c(t) + A(t)y^2 + B(t)y^4, \quad (3)$$

where the coefficients  $A(t)$  and  $B(t)$  are calculated by solving the ordinary differential equations

$$\begin{aligned} \frac{\gamma p_b}{\gamma - 1} \frac{d}{dt} \langle T \rangle &= -\frac{3\gamma p_b \dot{R}}{R} \langle T \rangle + \frac{6K}{R^2} \left\{ [2T_s + (\gamma - 2)\langle T \rangle] \right. \\ &\quad \times (A + 2B) - \frac{4}{5}A^2 - \frac{16}{9}B^2 - \frac{16}{7}AB \left. \right\}, \\ \frac{\gamma}{\gamma - 1} p_b \dot{T}_c &= \frac{3T_c}{R^2} [2(\gamma - 1)K(A + 2B) - \gamma p_b R \dot{R}] + \frac{6KT_c A}{R^2}, \end{aligned} \quad (4)$$

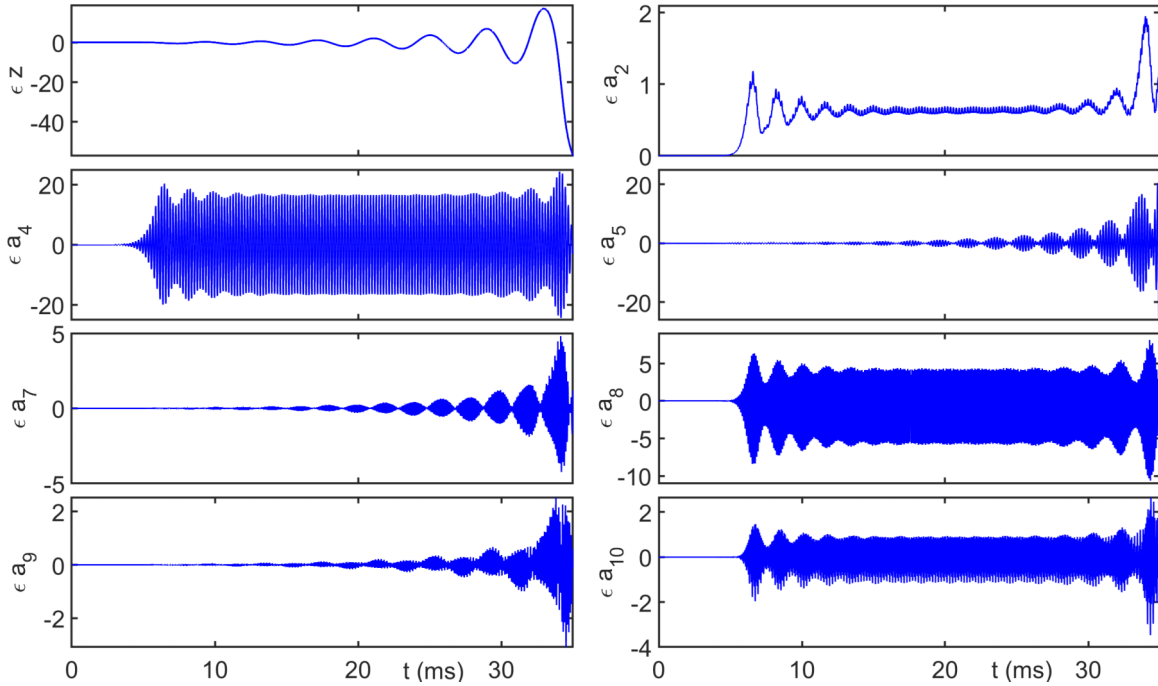


FIG. 3. Translation mode and shape mode oscillations for  $R_0 = 210 \mu\text{m}$ ,  $p_a = 11 \text{ kPa}$ , and  $f_d = 10 \text{ kHz}$ .

with the volume averaged gas temperature given by  $\langle T \rangle = T_c + 3A/5 + 3B/7$  and the (assumed) constant liquid temperature  $T_s = T_c + A + B$ . The temperature at the center of the bubble is denoted by  $T_c(t)$ , the ratio of specific heats by  $\gamma$  and the gas thermal conductivity by  $K$ . In order to calculate the corresponding gas pressure, mass conservation is applied to give

$$p_b(t) = \frac{p_{b0}}{3T_0\alpha} \left( \frac{R_0}{R(t)} \right)^3, \quad \text{where } \alpha = \int_0^1 \frac{y^2}{T} dy. \quad (5)$$

The subscript 0 denotes initial values while suitable analytic expressions for the integral  $\alpha$  are given in Ref. [25] depending on how  $A$ ,  $B$ , and  $T_c$  are related.

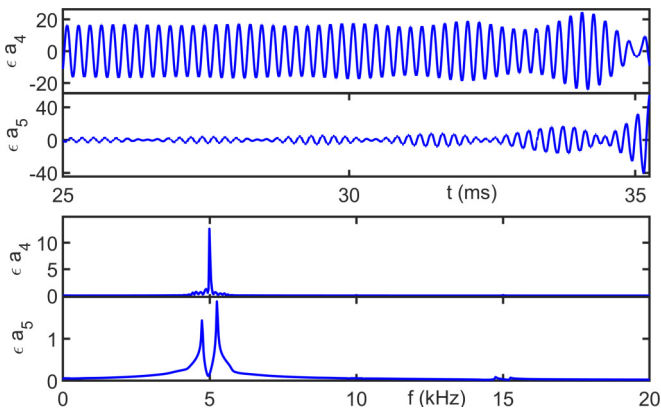


FIG. 4. Oscillations of the  $n=4$  and  $n=5$  shape modes on an enhanced timescale for  $R_0 = 210 \mu\text{m}$ ,  $p_a = 11 \text{ kPa}$ , and  $f_d = 10 \text{ kHz}$ , together with the corresponding amplitude frequency spectra.

### III. RESULTS AND DISCUSSION

Considering an air bubble in water at room temperature, the following set of parameters is used:  $T_s = 293.15^0 \text{ K}$ ,  $\gamma = 1.4$ ,  $K = 0.0259 \text{ Wm}^{-1}\text{K}^{-1}$ ,  $\rho = 998 \text{ kg m}^{-3}$ ,  $\mu = 0.001002 \text{ kg m}^{-1}\text{s}^{-1}$ ,  $p_0 = 101325 \text{ kg m}^{-1}\text{s}^{-2}$ ,

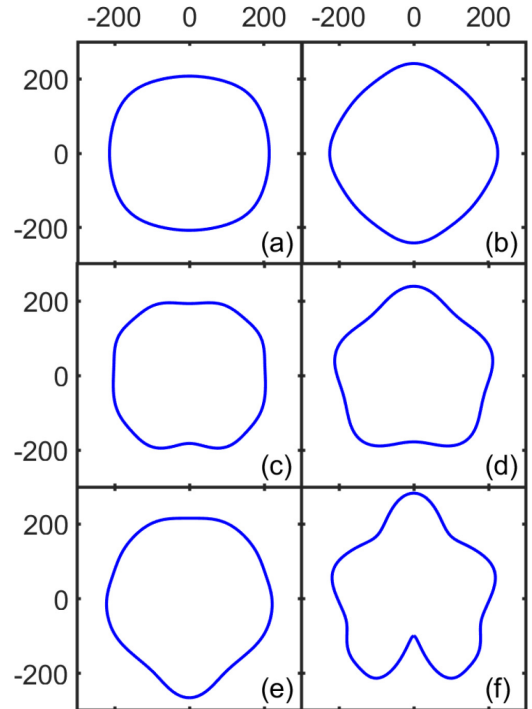


FIG. 5. Bubble shapes for  $R_0 = 210 \mu\text{m}$ ,  $p_a = 11 \text{ kPa}$ , and  $f_d = 10 \text{ kHz}$ . Plots (a)–(f) correspond to the respective times  $t = 5.97, 8.08, 34.34, 35.03, 35.17,$  and  $35.24 \text{ ms}$ .

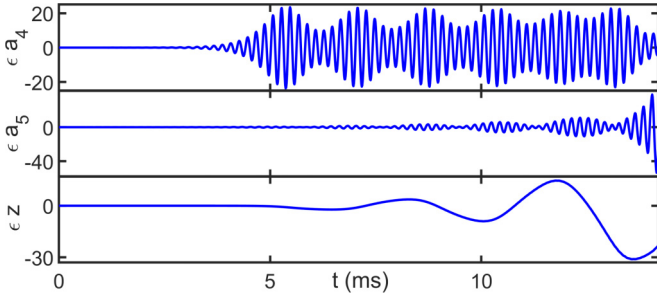


FIG. 6. Shape mode and translation evolutions for  $R_0 = 210 \mu\text{m}$ ,  $f_d = 10 \text{kHz}$ , and  $p_a = 11.5 \text{kPa}$ .

$c = 1500 \text{m s}^{-1}$ , and  $\sigma = 0.00728 \text{kg s}^{-2}$ , noting that  $\rho$  represents the liquid density,  $\mu$  the liquid dynamic viscosity,  $p_0$  the background ambient pressure in the liquid,  $c$  the speed of sound in the liquid, and  $\sigma$  the surface tension coefficient. Denoting the natural frequency of the  $n$ th axisymmetric shape mode by  $f_n$ , we are specifically interested in cases where two neighboring, axisymmetric shape modes are parametrically excited by the fundamental resonance for a given driving frequency, that is, cases where  $f_n$  and  $f_{n+1}$  are sufficiently close to the frequency  $2f_d$  that both modes are parametrically excited. As the order of the shape modes increases, the natural frequencies of the respective modes get closer together and therefore driving the system at intermediate frequencies, that is,  $2f_d$  is near the midpoint of the interval  $[f_n, f_{n+1}]$ , provided pertinent threshold values are exceeded, then it becomes more likely that two neighboring shape modes can both be excited by the fundamental resonance. To illustrate, the first set of results are for a bubble of initial radius  $R_0 = 210 \mu\text{m}$  and the driving frequency  $f_d = 10 \text{kHz}$ . We note that for  $R_0 = 189 \mu\text{m}$ , the predicted natural frequency of the  $n = 4$  mode is  $f_4 = 4.96 \text{kHz}$  while for  $R_0 = 230 \mu\text{m}$  the predicted natural frequency of the  $n = 5$  mode is  $f_5 = 5.05 \text{kHz}$  [26]. Therefore, the intermediate value  $R_0 = 210 \mu\text{m}$  is chosen as a good candidate for potential overlap, where we note that the respective estimated natural frequency values are  $f_4 = 4.24 \text{kHz}$  and  $f_5 = 5.79 \text{kHz}$ .

For a driving strength of  $p_a = 10 \text{kPa}$ , only the  $n = 4$  shape mode is predicted to undergo parametric excitation and this mode in turn excites other even shape modes through nonlinear shape mode interactions. In Fig. 1 the temporal evolution of the volume mode, the parametrically excited  $n = 4$  shape mode, and the shape mode with the next largest amplitude, the  $n = 8$  mode, are shown. The growth of the  $n = 4$  shape mode

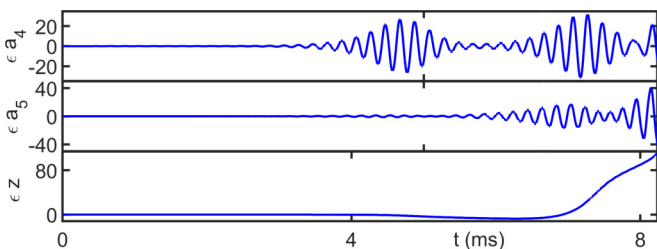


FIG. 7. Shape mode and translation evolutions for  $R_0 = 210 \mu\text{m}$ ,  $f_d = 10 \text{kHz}$ , and  $p_a = 12 \text{kPa}$ .

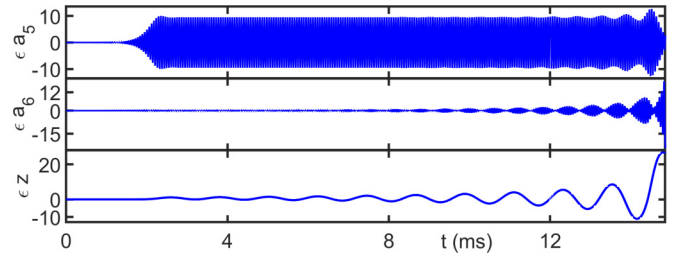


FIG. 8. Shape mode and translation evolutions for  $R_0 = 110 \mu\text{m}$ ,  $p_a = 5.3 \text{kPa}$ , and  $f_d = 35 \text{kHz}$ .

saturation and subsequently the bubble undergoes sustained, finite amplitude shape deformation consistent with previous observations for different parameter sets [12–17]. Plots of the volume mode and the  $n = 4$  shape mode on an enhanced timescale are shown in Fig. 2. Clearly the  $n = 4$  shape mode oscillates with a (dominant) frequency of  $5 \text{kHz}$ , indicating the parametric excitation is due to the fundamental resonance.

Increasing the driving pressure to  $p_a = 11 \text{kPa}$ , it is now found that both the  $n = 4$  and  $n = 5$  shape modes are parametrically excited as shown in Fig. 3, which displays the axial translation and the seven shape modes with the largest amplitudes. Enhanced timescale plots of the two parametrically excited shape modes are shown in Fig. 4 together with amplitude frequency spectra plots. Clearly the parametric excitation of the two shape modes occurs on different timescales. The  $n = 4$  shape mode is excited on a faster timescale with the initial exponential growth saturating and the shape mode then undergoing sustained, finite amplitude oscillations, with a dominant frequency of  $5 \text{kHz}$ . For the

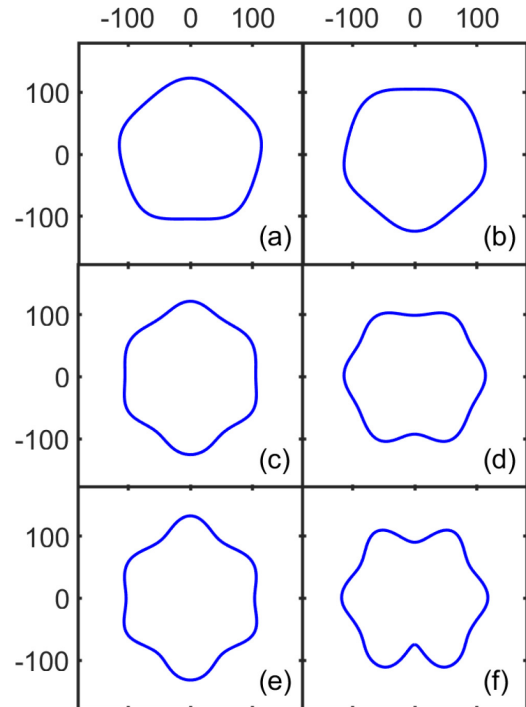


FIG. 9. Bubble shapes for  $R_0 = 110 \mu\text{m}$ ,  $p_a = 5.3 \text{kPa}$ , and  $f_d = 35 \text{kHz}$ . Plots (a)–(f) correspond to the respective times  $t = 9.95, 9.97, 14.77, 14.80, 14.83,$  and  $14.86 \text{ms}$ .

$n = 5$  shape mode, the parametrically induced growth occurs on a slower timescale, but the growth in this case is found not to saturate. Instead, the  $n = 5$  shape mode continues to grow in a modulated, exponential fashion. As the  $n = 5$  shape mode grows, modulations are also observed to develop in the  $n = 4$  shape mode oscillations. Spectral analysis of the  $n = 5$  shape mode reveals two dominant frequencies around, but not at, 5 kHz (the respective approximate values are 4.74 kHz and 5.25 kHz). In tandem with the growth of the  $n = 5$  shape mode, the bubble is also observed to move, with the resultant axial bubble displacement  $\epsilon z(t)$  displaying growing, periodic motion. In Fig. 5 sample bubble shapes are shown for the times indicated in the caption. In the latter stages a transition from the  $n = 4$  to  $n = 5$  dominated shape is clearly visible with a developing protrusion into the bubble noted in plot 5(f). This latter protrusion could indicate that subsequently the bubble splits or fragments, but such a predication goes beyond the present model. Note, both the translation mode and remaining shape modes shown in Fig. 3 are excited through nonlinear shape mode interactions.

In Figs. 6 and 7 plots of  $\epsilon a_4(t)$ ,  $\epsilon a_5(t)$ , and  $\epsilon z(t)$  are shown for  $p_a = 11.5$  kPa and  $p_a = 12$  kPa, respectively. Increasing the driving pressure results in the dynamics occurring on faster timescales, but the excitement in the  $n = 4$  shape mode still becomes observable first, with the resultant sustained, finite amplitude oscillations displaying distinct modulations. The resultant bubble translation is also seen to become more rapid, again with its growth coinciding with the observable, modulated growth in the  $n = 5$  shape mode.

These results would appear to be consistent with experimental observations. First, it is known that shape deforming bubbles are sensitive to positional instability and small increases in the driving pressure are sufficient to cause the shape deforming bubbles to move. Also, it is known that for a given driving pressure there can be a time delay between the bubble undergoing shape deformation and bubble self-propulsion being observed which is consistent with the neighboring shape modes being parametrically excited on different timescales. Therefore, for driving pressures just above the threshold for both shape modes to be parametrically excited, the bubble could undergo sustained, finite amplitude shape oscillations for a marked period of time before transitioning into a different shape mode oscillation configuration as the growth in the second shape mode becomes observable, and this will be accompanied by observable bubble motion.

This identified behavior type is found to be fairly generic when two neighboring shape modes are parametrically excited via the first parametric resonance. To illustrate, Fig. 8 displays the temporal evolution of the parametrically excited shape modes  $n = 5$  and  $n = 6$  together with the bubble displacement for  $R_0 = 110 \mu\text{m}$ ,  $p_a = 5.3$  kPa, and  $f_d = 35$  kHz, where again the development of the shape modes on different timescales is clear. Note, other shape modes are again excited nonlinearly through shape mode interactions, this being key, as already noted, to the shape mode excited on the faster timescale attaining sustained, finite amplitude oscillations and therefore in turn to permit the observable development of the other parametrically excited shape mode. Corresponding selected bubble shapes are shown in Fig. 9 where a transition from the  $n = 5$  to the  $n = 6$  dominated shape is seen. In

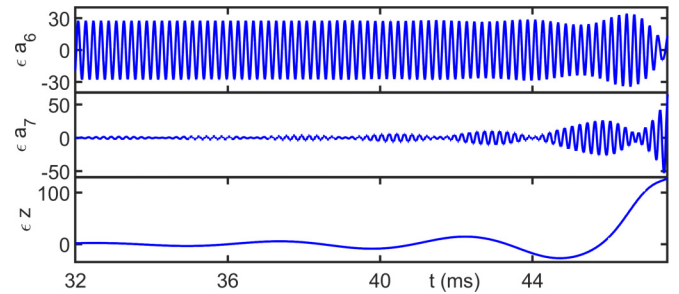


FIG. 10. Shape mode and translation evolutions for  $R_0 = 295 \mu\text{m}$ ,  $p_a = 1.75$  kPa, and  $f_d = 10$  kHz.

Fig. 10, plots of the later stages of the temporal development of the parametrically excited  $n = 6$  and  $n = 7$  shapes modes together with the bubble displacement for  $R_0 = 295 \mu\text{m}$ ,  $p_a = 1.75$  kPa, and  $f_d = 10$  kHz are displayed. Finally, in Fig. 11, plots of the parametrically excited neighboring shape modes  $n = 7$  and  $n = 8$  and the bubble displacement  $\epsilon z(t)$  are shown for  $R_0 = 134 \mu\text{m}$ ,  $p_a = 13$  kPa, and  $f_d = 40$  kHz with corresponding amplitude spectrum plots for the shape modes being shown in Fig. 12. We note that all of the presented parametrically excited shape modes have been excited via the fundamental resonance and the results are consistent with the previous observations.

Finally, we note that for the neighboring pairs  $n = 2$ ,  $n = 3$  and  $n = 3$ ,  $n = 4$ , the natural frequencies of the respective shape modes are sufficiently far apart that a suitable intermediate value is more difficult to find where the two neighboring shape modes are excited via the fundamental resonance. Instead, higher parametric resonances are more likely to occur at intermediate values.

#### IV. CONCLUSIONS

In this work we have considered the parametric excitement of two neighboring shape modes at the same driving frequency via the fundamental resonance mechanism. For a sufficiently large shape mode number, and provided a pertinent driving pressure threshold value is exceeded, the two shape modes are found to grow on different timescales. The growth of the shape mode on the faster timescale is found to saturate and then subsequently undergo sustained, finite amplitude oscillations as a consequence of the nonlinear excitement of other shape modes. The growth of the shape mode

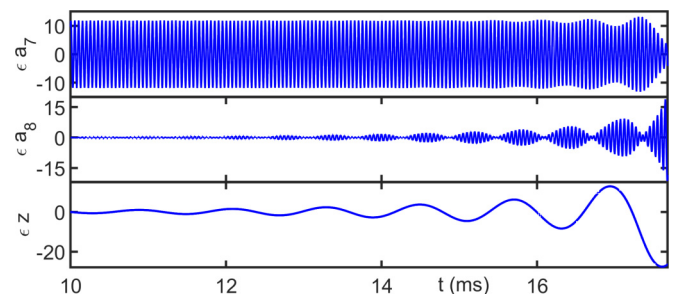


FIG. 11. Shape mode and translation evolutions for  $R_0 = 134 \mu\text{m}$ ,  $p_a = 13$  kPa, and  $f_d = 40$  kHz.

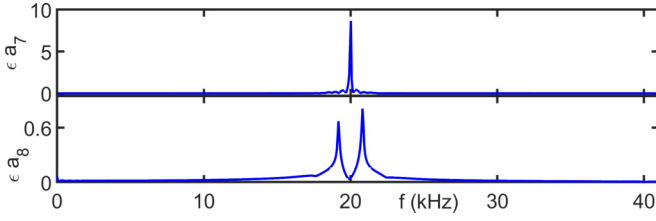


FIG. 12. Amplitude frequency spectra for the  $n = 7$  and  $n = 8$  shapes modes for  $R_0 = 134 \mu\text{m}$ ,  $p_a = 13 \text{ kPa}$ , and  $f_d = 40 \text{ kHz}$ .

on the slower timescale is found to be both modulated and unbounded. Concurrent with the growth of this shape mode, oscillatory, growing bubble translation is also observed. Increasing the driving pressure causes events to occur on faster timescales, but the development of the neighboring shape modes remains distinct. The presented results would appear

to be consistent with experimental observation in that for a bubble undergoing shape deformation only a small increase in the driving pressure is sufficient to cause positional instability. This is directly linked to the necessary threshold driving pressure for parametric excitation being exceeded for both neighboring shape modes. Also, for a given driving strength a time delay can occur between the bubble being observed to deform in shape and the bubble being observed to move. This can be explained by the development of the respective parametrically excited shape modes on different timescales.

### APPENDIX: DYNAMICAL EQUATIONS

The equations employed to model the volume mode  $R(t)$ , translation mode  $\epsilon z(t)$ , and the shape modes  $\epsilon a_n(t)$ ,  $n \geq 2$  in condensed form are the following: for the volume mode,

$$\begin{aligned}
 R\ddot{R}\left(1 - \frac{2\dot{R}}{c}\right) + \frac{3}{2}\dot{R}^2\left(1 - \frac{4\dot{R}}{3c}\right) = G + \frac{R}{c}\dot{G} + \epsilon^2 \frac{u^2}{4} + \epsilon^2 \sum_{n=2}^{\infty} \frac{1}{(2n+1)(n+1)} \left[ (n-3) \left( \frac{\dot{R}a_n^2}{R} + \frac{\dot{R}^2 a_n^2}{2R^2} + \frac{2\dot{R}a_n\dot{a}_n}{R} \right) \right. \\
 \left. - \left( n + \frac{3}{2} \right) \dot{a}_n^2 - (n+3)a_n\ddot{a}_n \right] + \epsilon^2 \frac{\mu}{\rho} \sum_{n=2}^{\infty} \frac{2}{(2n+1)(n+1)} \left[ \frac{4n^2\dot{R}}{R^3} a_n^2 - (n^2 + 5n + 2) \frac{a_n\dot{a}_n}{R^2} \right] \\
 + \epsilon^2 \frac{(p_b - p_\infty)}{\rho} \sum_{n=2}^{\infty} \frac{a_n^2}{(2n+1)R^2} + \epsilon^3 f_0(t), \tag{A1}
 \end{aligned}$$

where

$$G(t) = \frac{(p_b - p_\infty)}{\rho} - \frac{4\mu\dot{R}}{\rho R} - \frac{2\sigma}{\rho R}, \tag{A2}$$

while for the axial bubble translation

$$\begin{aligned}
 \epsilon \left[ R\ddot{z} + 3\dot{R}\dot{z} + \frac{18\mu}{\rho R}\dot{z} \right] = \epsilon^2 \frac{9}{5} a_2 \ddot{z} + \epsilon^2 \left( \frac{9}{5} \dot{a}_2 + \frac{18\dot{R}}{5R} a_2 \right) \dot{z} \\
 + \epsilon^2 \sum_{n=2}^{\infty} \frac{9}{(2n+1)(n+1)} \left[ 2na_n a_{n+1} \left( \frac{\dot{R}^2}{R^2} + \frac{\ddot{R}}{R} \right) - (n+1)\ddot{a}_{n+1} a_n - \dot{a}_{n+1} \dot{a}_n + n\ddot{a}_n a_{n+1} \right. \\
 \left. - \frac{2\dot{R}}{R} (\dot{a}_{n+1} a_n - 2n\dot{a}_n a_{n+1}) \right] + \epsilon^2 \frac{36\mu a_2}{\rho R^2} \dot{z} \\
 + \epsilon^2 \frac{\mu}{\rho} \left\{ \sum_{n=2}^{\infty} \frac{18n(n+1)}{(2n+1)(2n+3)} \left[ \frac{9\dot{R}}{R^3} a_n a_{n+1} + 2(n+2) \frac{\dot{a}_n a_{n+1}}{R^2} \right] - \sum_{n=3}^{\infty} \frac{18n(2n^2+1)}{(4n^2-1)} \frac{\dot{a}_n a_{n-1}}{R^2} \right\}, \\
 + \epsilon^3 f_1(t), \tag{A3}
 \end{aligned}$$

and for the amplitude of the  $n$ th shape mode

$$\begin{aligned}
 \epsilon \left\{ R\ddot{a}_n + 3\dot{R}\dot{a}_n + (n^2 - 1)(n+2) \frac{\sigma}{\rho R^2} a_n - (n-1)\ddot{R}a_n + \frac{2\mu}{\rho} \left[ (n-1)(n+2) \frac{\dot{R}}{R^2} a_n + (n+2)(2n+1) \frac{\dot{a}_n}{R} \right] \right\} \\
 = -\epsilon^2 \frac{9}{4} \delta_{2n} u^2 + \epsilon^2 \left[ \frac{3n(n+1)}{2(2n+3)} \ddot{z} a_{n+1} + \frac{3(n+1)(2n+1)}{2(2n+3)} \dot{z} \dot{a}_{n+1} \right] \\
 - \epsilon^2 (1 - \delta_{2n}) \left[ \frac{3n(n+1)}{2(2n-1)} \ddot{z} a_{n-1} + \frac{3(n+1)\dot{R}}{R} \dot{z} a_{n-1} + \frac{3}{2} (n+1) \dot{z} \dot{a}_{n-1} \right] \\
 - \epsilon^2 \sum_{i=2}^{\infty} \sum_{j=2}^{\infty} \frac{(2n+1)(n+1)}{4} \left[ \frac{\ddot{R}}{R} a_i a_j G_{d_{ijn}} + \frac{\dot{R}^2}{R^2} a_i a_j M_{a_{nij}} + \frac{\dot{R}}{R} \dot{a}_j a_i M_{b_{nij}} + a_i \ddot{a}_j M_{c_{nij}} + \dot{a}_i \dot{a}_j M_{d_{nij}} \right]
 \end{aligned}$$

$$\begin{aligned}
& + \epsilon^2 \frac{\mu}{\rho} \left[ \frac{6n(n+1)^2(n+2)}{(2n+3)} \frac{\dot{z}a_{n+1}}{R^2} - (1 - \delta_{2n}) \frac{3n(n+1)(2n^2+1)}{(2n-1)} \frac{\dot{z}a_{n-1}}{R^2} \right] \\
& + \epsilon^2 \frac{\mu}{\rho} \sum_{i=2}^{\infty} \sum_{j=2}^{\infty} \frac{(2n+1)(n+1)}{4} \left[ \frac{\dot{a}_j a_i}{R^2} (Q_{b_{nij}} + Q_{b_{jin}}) + \frac{\dot{R}}{R^3} a_i a_j Q_{c_{jin}} \right] \\
& + \frac{(p_b - p_{\infty})}{2\rho} \epsilon^2 \sum_{i=2}^{\infty} \sum_{j=2}^{\infty} (2n+1)(n+1) I_{a_{nij}} \frac{a_i a_j}{R^2} + \epsilon^3 f_n(t). \tag{A4}
\end{aligned}$$

Within this system  $p_{\infty} = p_0 + p_a \sin(2\pi f_d t)$ ,  $p_a$  denotes the driving pressure,  $f_d$  the driving frequency,  $p_0$  the background ambient pressure in the surrounding liquid,  $\rho$  the density of the liquid,  $\mu$  the liquid dynamic viscosity,  $\sigma$  the surface tension coefficient, and  $\delta_{ij}$  the Kronecker delta. The coefficients  $G_{d_{ijn}}$ ,  $M_{a_{nij}}$ ,  $M_{b_{nij}}$ ,  $M_{c_{nij}}$ ,  $M_{d_{nij}}$ , and  $I_{a_{nij}}$  are defined in the Appendix of Shaw [20] while the viscous coefficients  $Q_{b_{nij}}$  and  $Q_{c_{jin}}$  are defined in the Appendix of Shaw [21]. These coefficients all involve different combinations of integrated Legendre polynomial products. For brevity of presentation, the terms at cubic order in  $\epsilon$  are not repeated here but are instead denoted by the set of terms  $\epsilon^3 f_i(t)$ ,  $i \geq 0$ . Their full form can be found in Refs. [20,21].

- 
- [1] H. Lamb, *Hydrodynamics*, 4th ed. (Cambridge University Press, Cambridge, 1916).
- [2] N. Gaines, A magnetostriction oscillator producing intense audible sound and some effects obtained, *Physics* **3**, 209 (1932).
- [3] J. Janiak, Y. Li, Y. Ferry, A. A. Doinikov, and D. Ahmed, Acoustic microbubble propulsion, train-like assembly and cargo transport, *Nat. Commun.* **14**, 4705 (2023).
- [4] M. Strasberg and T. B. Benjamin, Excitation of oscillations in the shape of pulsating gas bubbles; experimental work (abstract), *J. Acoust. Soc. Am.* **30**, 697 (1958).
- [5] T. B. Benjamin and M. Strasberg, Excitation of oscillations in the shape of pulsating gas bubbles; theoretical work (abstract), *J. Acoust. Soc. Am.* **30**, 697 (1958).
- [6] L. A. Crum and A. I. Eller, Motion of bubbles in a stationary sound field, *J. Acoust. Soc. Am.* **48**, 181 (1970).
- [7] T. B. Benjamin and A. T. Ellis, Self-propulsion of asymmetrically vibrating bubbles, *J. Fluid Mech.* **212**, 65 (1990).
- [8] P. G. Saffman, The self-propulsion of a deformable body in a perfect body, *J. Fluid Mech.* **28**, 385 (1967).
- [9] C. C. Mei and X. Zhou, Parametric resonance of a spherical bubble, *J. Fluid Mech.* **229**, 29 (1991).
- [10] Z. C. Feng and L. G. Leal, Translation instability of a bubble undergoing shape oscillations, *Phys. Fluids* **7**, 1325 (1995).
- [11] A. A. Doinikov, Translational motion of a bubble undergoing shape oscillations, *J. Fluid Mech.* **501**, 1 (1999).
- [12] M. Guédra, C. Inserra, B. Gilles, and C. Mauger, Periodic onset of bubble shape instabilities and their influence on the spherical mode, in *IEEE International Symposium Proceedings* (IEEE, New York, USA, 2016), pp. 1–4.
- [13] M. Guédra, C. Inserra, C. Mauger, and B. Gilles, Experimental evidence of nonlinear mode coupling between spherical and nonspherical oscillations of microbubbles, *Phys. Rev. E* **94**, 053115 (2016).
- [14] M. Guédra, S. Cleve, C. Mauger, P. Blanc-Benon, and C. Inserra, Dynamics of nonspherical microbubble oscillations above instability threshold, *Phys. Rev. E* **96**, 063104 (2017).
- [15] S. J. Shaw, Nonspherical sub-millimeter gas bubble oscillations: Parametric forcing and nonlinear shape mode coupling, *Phys. Fluids* **29**, 122103 (2017).
- [16] M. Guédra and C. Inserra, Bubble shape oscillations of finite amplitude, *J. Fluid Mech.* **857**, 681 (2018).
- [17] S. Cleve, M. Guédra, C. Inserra, C. Mauger, and P. Blanc-Benon, Surface modes with controlled axisymmetry triggered by bubble coalescence in a high-amplitude acoustic field, *Phys. Rev. E* **98**, 033115 (2018).
- [18] A. Francescutto and R. Nabergoj, Pulsation amplitude threshold for surface waves on oscillating bubbles, *Acustica* **41**, 215 (1978).
- [19] M. Versluis, D. E. Goertz, P. Palanchon, I. L. Heitman, S. M. van der Meer, B. Dollet, N. de Jong, and D. Lohse, Microbubble shape oscillations excited through ultrasonic parametric driving, *Phys. Rev. E* **82**, 026321 (2010).
- [20] S. J. Shaw, Translation and oscillation of a bubble under axisymmetric deformation, *Phys. Fluids* **18**, 072104 (2006).
- [21] S. J. Shaw, The stability of a bubble in a weakly viscous liquid subject to an acoustic travelling wave, *Phys. Fluids* **21**, 022104 (2009).
- [22] A. Prosperetti, Thermal effects and damping mechanisms in the forced radial oscillations of gas bubbles in liquids, *J. Acoust. Soc. Am.* **61**, 17 (1977).
- [23] A. Prosperetti, L. A. Crum, and K. W. Commander, Nonlinear bubble dynamics, *J. Acoust. Soc. Am.* **83**, 502 (1988).
- [24] A. Prosperetti, The thermal behaviour of oscillating gas bubbles, *J. Fluid Mech.* **222**, 587 (1991).
- [25] G. Zhou and A. Prosperetti, Modelling the thermal behaviour of gas bubbles, *J. Fluid Mech.* **901**, R3 (2020).
- [26] The natural frequency values of the shape modes are estimated using the formula of Lauterborn [27] modified to include the thermal dissipation term of Prosperetti [22] and where the polytropic index is estimated using the corresponding equation also given by Prosperetti [22].
- [27] W. Lauterborn, Numerical investigation of nonlinear oscillations of gas bubbles in liquids, *J. Acoust. Soc. Am.* **59**, 283 (1976).